REVIEW ARTICLE

Fracture Mechanics of Cement Mortar and Plain Concrete

B.L. Karihaloo, A. Carpinteri, and M. Elices
School of Civil and Mining Engineering, The University of Sydney, Australia, Dipartimento di Ingegneria Strutturale, Politechnico di Torino, Torino, Italy, and Departamento de Ciencia de Materiales, Universidad Politecnica de Madrid, Ciudad Universitaria, Madrid

The classical Griffith theory is modified to include the prepeak nonlinear and postpeak tension-softening response of cement mortar and concrete. This is done through the notion of an equivalent (effective) brittle material which permits the calculation of the real fracture energy G_F of the material. The latter is used to explain the ductile-brittle transition via the (energy) brittleness number. A simplified procedure for studying the crack growth in cement mortar and plain concrete is formulated on the basis of an equivalent elastic material, and its limitations are pointed out. ADVANCED CEMENT BASED MATERIALS 1993, 1, 92–105

KEY WORDS: Elastic equivalences, Energy brittleness number, Equivalent (effective) brittle material, Modified Griffith theory, Tension-softening

The last decade has improved our understanding of the role of defects such as pores and cracks in the tensile response of the cement based materials that were traditionally regarded as being brittle. It is now generally accepted that all cement based materials exhibit moderate strain hardening prior to the attainment of their ultimate tensile capacity (region AB in Figure 1), reminiscent of the response of high-strength metallic materials. However, unlike the latter, these materials are characterized by an increase in deformation with decreasing tensile capacity past the ultimate strength (region BCD in Figure 1). Such a response is called tension softening. The materials exhibiting moderate strain hardening prior to the attainment of ultimate tensile strength and tension softening thereafter may be called quasibrittle. It was precisely because of such behavior that the classical linear elastic fracture mechanics (LEFM) was found to be inadequate for such materials, although attempts were made in the 1950s [1–4]. A modification of the classical LEFM was achieved through the so-called cohesive crack model in which the real, open macrocrack was assumed to terminate in a zone with a residual stress transfer capability (fracture process zone) [5] and the corresponding toughness (fracture energy) was designated G_F. The practical use of cohesive crack model relies on sophisticated numerical procedures that are often cumbersome. The existence of a fracture process zone ahead of a macrocrack also results in a size effect whereby the larger the size of the object the more brittle its observed response.

This article will first describe a direct modification of the classical Griffith theory by the inclusion of prepeak nonlinear and postpeak tension-softening response and introduce the notion of an equivalent (effective) brittle material. This will help in the direct calculation of the real fracture energy G_F of cement mortar and plain concrete. It will then explain the ductile-brittle transition based on the notion of (energy) brittleness number $s_e = G_F/(f_t D)$, where f_t is the ultimate tensile strength of the material and D a characteristic structural dimension. Finally, it will present a simplified procedure for evaluating crack growth in cement mortar and plain concrete based on a general concept of an equivalent elastic material, pointing out the limitations of this concept.

Prepeak and Postpeak Nonlinear Response

All cement based materials contain pores and microcracks even in their virgin, unstressed state. Under applied tensile stresses, microcracks form at the mortar/aggregate interfaces leading to the prepeak nonlinearity. The transition from linear to nonlinear response (point A Figure 1) is primarily governed by the extent of available interfaces.

For cement mortar and plain concrete, the threshold and ultimate strains were accurately measured by Kaplan [6] under several tensile loading combinations. He found that they depend on only the volume fraction of the coarse aggregate in the mix, but do not vary with other microstructural parameters, such as the type and texture of coarse aggregate or the water:cement ratio.

The interfacial microcracks first form between the

Address correspondence to: B.L. Karihaloo, School of Civil and Mining Engineering, The University of Sydney, NSW 2006, Australia.

ISSN 1065-7355/93/$6.00

Received July 28, 1993
Accepted September 7, 1993

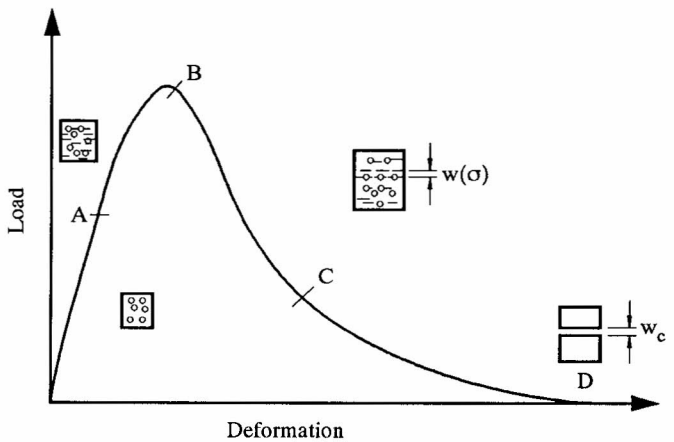

FIGURE 1. Typical load-deformation response of a cement based material in tension showing (1) the transition from linear to nonlinear response (point A); (2) prepeak nonlinearity (AB); (3) onset of localization of deformation (point B); and (4) postpeak tension-softening response (BCD).

mortar and the largest size aggregates. With a further increase in tensile stress, not only do the existing microcracks propagate stably, but also more microcracks are progressively formed at interfaces between the mortar and aggregates of smaller size. As cement based materials usually contain a range of aggregate size, the process of stable microcrack growth and formation of new microcracks continues under increasing tensile stress resulting in the prepeak nonlinearity (stage AB in Figure 1).

This prepeak nonlinear response has been accurately explained using damage mechanics models (see, e.g., ref 7). These models are applicable when the microcracks are evenly distributed and are not too numerous. However, even after the deformation has begun to localize near the eventual fracture plane (point B in Figure 1), fracture does not immediately follow. Point B could even lie on the ascending branch. The decreasing stress transfer capacity with increasing deformation in the tension-softening regime is a result of the progressive rupture of the intact ligaments that break the continuity of flaws. Because this progressive microdamage consumes energy, the intrinsic toughness of quasibrittle materials is improved. Further improvement of toughness is achieved by external means, such as fiber reinforcement, but this toughening mechanism will not be pursued here.

Several two- and three-dimensional models have been proposed to describe the tension-softening behavior of quasibrittle materials. The two-dimensional model considered first by Horii et al. [8] and later by Ortiz [9] treats the discontinuous macroflaw as a row of collinear cracks subjected to a normal tensile stress well removed from the line of cracks. This model predicts unstable rupture when the inelastic deformation attains a critical value. Such unstable behavior, however, is not a material response but is a result of the model assuming the cracks will coalesce, which may not happen. In fact, it would seem (Melin [10]) that when the tips of adjacent straight cracks approach so close to each other that the straight path would be unstable, they avoid each other by curving and form "eyelets" in the process. Such crack curving and formation of eyelets have been repeatedly observed in tension tests on cement mortar and concrete specimens [11].

The tension-softening response of most cement based materials is characterized by a pronounced tail [12], which has been predicted by the two-dimensional model of Karihaloo et al. [13]. In this model, the discontinuous macroflaw is treated as a row of collinear cracks interspersed by circular pores and unbroken ligaments. The three-dimensional model of Li and Huang [14] regards the discontinuous macroflaw as consisting of a row of penny-shaped cracks separated by the largest second-phase particles (assumed as circular disks) in the matrix, so that neighboring cracks do not interact. However, as the tension-softening implies progressive approach of the neighboring broken segments toward each other, their interaction cannot be ignored. In the three-dimensional model of ref 15, the discontinuous macroflaw is modeled by a singly or doubly periodic array of penny-shaped cracks in the eventual fracture plane, allowing for full interactions between the cracks.

In both the two- and three-dimensional models a relationship between the decreasing stress transfer capacity, σ, the average net inelastic opening across the discontinuous fracture plane, w, as a function of the increasing damage parameter, γ, is obtained

$$\frac{\sigma}{f_t} = F_1(\gamma),\ w = F_2(\gamma). \tag{1}$$

$F_1(\gamma)$ and $F_2(\gamma)$ are determined from the solution of the boundary value problem corresponding to the chosen model [8,9,13–15], and the microscopic ultimate tensile strength f_t is related to $F_1(\gamma_o)$ and the matrix fracture toughness K_{Ic}^m, that is, the intrinsic crack growth resistance of cement paste. γ_o is the (small) accumulated damage at the onset of tension softening, that is, it reflects the prepeak nonlinearity. Examples of tension-softening diagrams obtained using the model of ref 13 are shown in Figure 2.

Effective Griffith Crack Concept

As mentioned above, for cement mortar and plain concrete, the classical Griffith approach to brittle materials

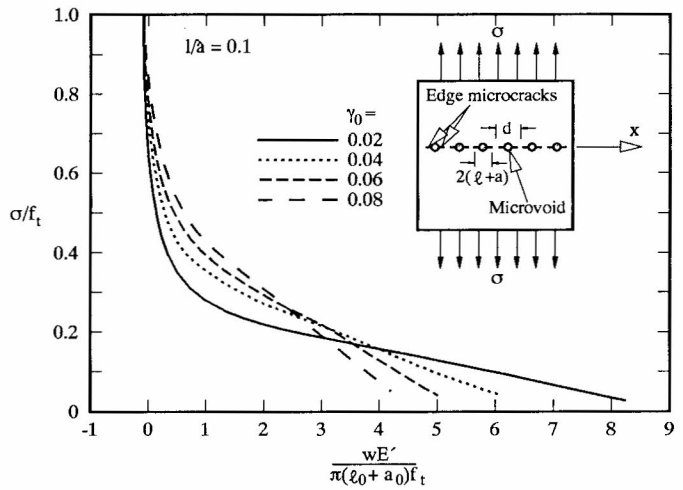

FIGURE 2. Tension-softening curves predicted by the model shown in the inset for various values of initial damage (including the circular pores).

has to be modified to account for the prepeak nonlinearity and the postpeak tension softening, that is, for the energy expended on microdamage rather than on the creation of critical fracture surfaces (critical macrocrack). This diffuse zone of microdamage is commonly called the process zone.

A modification based on the concept of an equivalent (or effective) crack was proposed by Jenq and Shah [16] and Nallathambi and Karihaloo [17], who used the classical Griffith theory but with the size of any precrack augmented to account for the energy expended in the process zone. [Here it is worth recalling that test specimens used to determine fracture toughness K_{Ic} and/or critical energy release rate G_{Ic} are usually provided with a well-defined sharp starter crack (length a_o) from which it is easier to study the instability phenomenon.] It was reasoned that the energy expended in the process zone can be equated to that required to create a fictitious (traction-free) crack (Figure 3). In practice, though, the length of the latter was determined not from the indicated energy balance but rather by comparing either the compliances [16] or the stiffnesses [17]. The size of the supplementary fictitious crack so calculated is designated by Δa or Δa_e and the corresponding fracture toughness K^s_{Ic} or K^e_{Ic} to distinguish it from the fracture toughness K_{Ic} of an ideally brittle material. It will be noted that in this modified Griffith approach the instability condition in quasibrittle materials is governed by two parameters [K^S_{Ic} and $a = a_o + \Delta a$ (or the critical crack opening corresponding to it) in the two-parameter model of Shah and Jenq [16]; K^e_{Ic} and $a_e = a_o + \Delta a_e$ in the effective crack model of Karihaloo and Nallathambi [18]), as opposed to just one parameter (K_{Ic}) in brittle materials.

The procedures for determining K^s_{Ic} and K^e_{Ic} are summarized in ref 18 and will not be repeated here. We note en passant that for normal age concrete, K^e_{Ic} and K^s_{Ic} increase with increasing f_t, whereas Δa_e and Δa depict the opposite trend. Thus, it is Δa_e or Δa rather than K^e_{Ic} or K^s_{Ic} which defines the brittleness of a cement based material; the higher the tensile strength, f_t, the lower Δa_e or Δa for structures of identical geometry. This situation is unlike that in metals for which the fracture toughness decreases with increasing tensile strength.

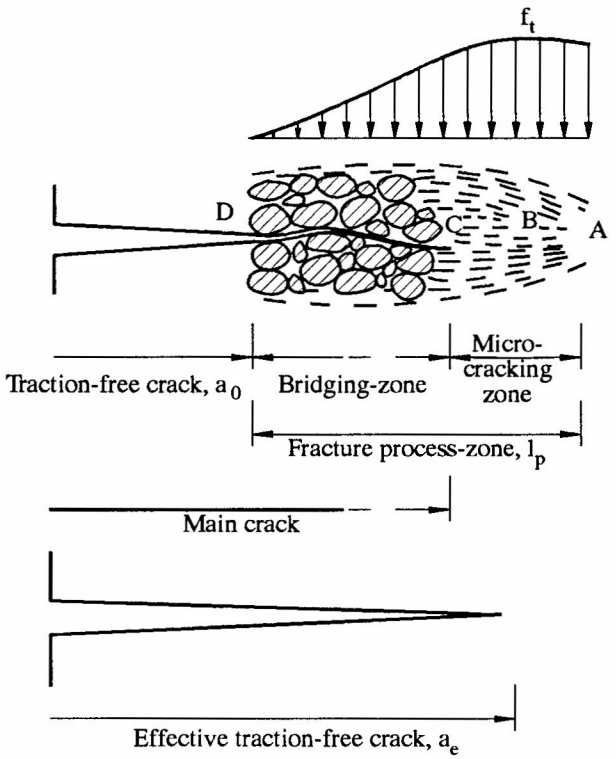

FIGURE 3. Process zone ahead of real traction-free crack and the concept of effective traction-free crack.

From the previous micromechanical models for tension softening it is possible to calculate the energy required for complete fracture of the material. This energy per unit area, denoted G_F, is given by the area under the curve shown, for example, in Figure 2

$$G_F = \int_{f_t}^{o} w(\sigma)d\sigma \equiv \int_{o}^{w_c} \sigma(w)dw \qquad (2)$$

where $\sigma(w)$ defines the tension softening and is a function of the accumulated damage at the onset of deformation localization (eq 1). In practice, G_F is determined from tests conducted in various loading geometries (e.g., three-point bending [19]), but this value may grossly overestimate the real fracture energy because it includes energy expended on processes other than the

formation of fracture surfaces, for example on cracking in the bulk of the specimen, etc.

The area under the tension-softening curve (eq 1) between the limits $\gamma_o \leq \gamma \leq 1$ gives the real fracture energy

$$G_F = \int_{f_t}^{o} w(\sigma)d\sigma \equiv \int_{\gamma_o}^{1} w(\gamma)\frac{\partial\sigma}{\partial\gamma}d\gamma. \quad (3)$$

The energy G_F (per unit area) expended on the creation of a traction-free crack of relative length $(1 - \gamma_o)$ at complete rupture can now be used to put the effective fracture toughness K_{Ic}^e, actually the effective toughness G_{Ic}^e corresponding to it ($G_{Ic}^e = (K_{Ic}^e)^2/E'$), on a firm physical footing simply by equating the total energies (per unit thickness)

$$\begin{aligned} G_F &= G_{Ic}^e(1 - \gamma_o) \\ &= (K_{Ic}^e)^2(1 - \gamma_o)/E'. \end{aligned} \quad (4)$$

The toughening ratio K_{Ic}^e/K_{Ic}^m can be shown to be [13–15,20]

$$K_{Ic}^e/K_{Ic}^m = F_3(\gamma;\gamma_o) \quad (5)$$

where F_3 $(\gamma;\gamma_o)$ is again determined from the solution of the corresponding boundary value problem.

Figure 4 shows the ratio of the effective fracture toughness K_{Ic}^e to the matrix fracture toughness K_{Ic}^m (eq 5) for several levels of the accumulated damage at peak load γ_o as a function of the parameter β. The latter in this model [13] is a measure of the relative fractions of microvoids and microcracks. Thus, $\beta = 0$ denotes the absence of microvoids, whereas $\beta \approx 1$ implies microvoids with negligibly small edge microcracks. The curves in Figure 4 are reminiscent of the classical creep curves, with an initial primary region of increasing K_{Ic}^e/K_{Ic}^m with increasing $\beta < 0.15$, an intermediate secondary or steady-state region for $0.15 \leq \beta \leq 0.60$ in which K_{Ic}^e/K_{Ic}^m remains practically constant, and a tertiary region in which this ratio increases sharply with increasing $\beta > 0.6$. The variation of K_{Ic}^e/K_{Ic}^m with γ_o for a fixed β is fairly moderate (Figure 5). It is evident that microcracks alone cannot make a large contribution to the toughening of quasibrittle materials. For further illustration, we write explicitly the toughening ratio from eq 5 for the two extreme cases of $\beta = 0$ (no microvoids) and $\beta \approx 1$ (microvoids with negligibly small edge microcracks), using the appropriate coefficients

$$K_{Ic}^e/K_{Ic}^m = \begin{matrix} 1.0039 + 0.3265\gamma_o \ (\beta = 0) \\ 1.7360 + 0.6732\gamma_o \ (\beta \approx 1) \end{matrix} \quad (6)$$

Thus, for a material such as high-strength concrete, even when the accumulated damage (including any preexisting damage) at peak load is large ($\gamma_o = 0.25$, say), the toughening provided by this mechanism ($\beta = 0$ in eq 6) would be just 8.5%. Concretes of normal strength and cement mortars, though, can be expected to have a β value in the range of $0.15 \leq \beta \leq 0.6$, so that the toughening provided by the tension softening would range between 15% and 20% (Figure 5) depending on the damage present at peak load.

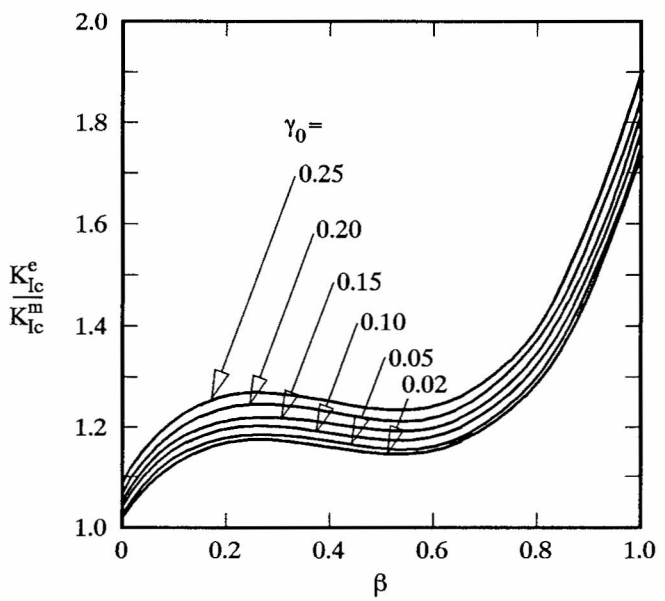

FIGURE 4. Variation of the toughening ratio with β for several levels of the accumulated damage at peak load, γ_o.

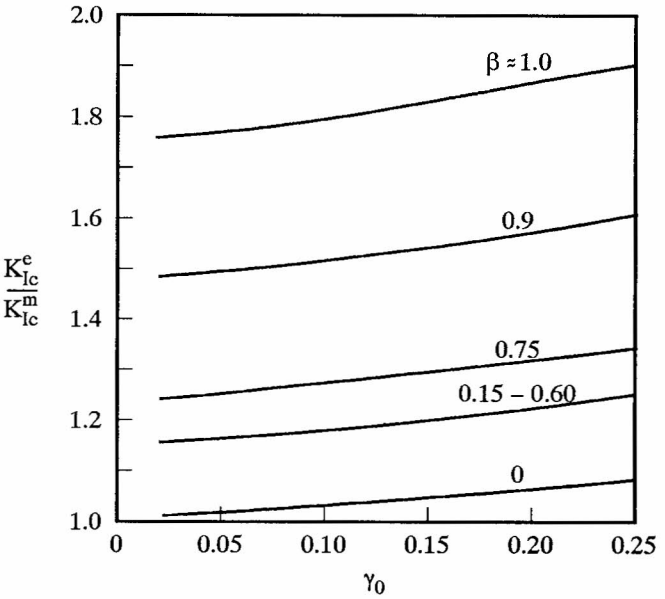

FIGURE 5. Variation of the toughening ratio with γ_0 for various relative fractions of microvoids and microcracks (β).

Advn Cem Bas Mat
1993;1:92–105

To complete this section, it may be pointed out that the damage accumulated in concrete at peak load (γ_o) depends only on the volume fraction of the coarse aggregate V_f [6]. It follows therefore from eq 5 that K_{Ic}^e can be expressed in terms of only K_{Ic}^m and V_f (in the range $0.15 \leq \beta \leq 0.6$), that is, a similar dependence to that predicted by the tension-softening model for concrete proposed in ref 14.

A comparison of the effective fracture toughness K_{Ic}^e calculated above from a micromechanical point of view with the fracture toughness obtained using the effective crack model [18] clearly demonstrates that supplementary fictitious traction-free crack Δa_e is a measure of the brittleness of the cement based material. The smaller its value, the more brittle the material. In fact, the microscopic parameters f_t and γ_o can be expressed in terms of K_{Ic}^e and Δa_e [21], so that we can define brittleness using the effective crack concept.

Ductility Size Effects

From a practical point of view, an approach based on the concept of brittleness number has been found to be more useful. Brittleness is often confused with low material strength. The two properties are in fact entirely distinct. Materials can be strong but brittle (glass, ceramics, cast iron, etc.) and they can be weak but tough (concrete, rock, wood, etc.). Brittleness is the tendency to break suddenly and noisily but not necessarily at low stresses.

One of the most significant discoveries in recent years in the field of Structural Engineering was that the brittleness of structural elements depends on their size. Small elements fail in a ductile or plastic manner, while large elements of the same material fail in a brittle or catastrophic manner. This can be explained by the fact that the two intrinsic properties of the material, namely the strength and toughness, have different physical dimensions: strength is force per unit area, that is, energy per unit volume, while toughness is force per unit of length, that is, energy per unit area. It is possible to demonstrate that the brittleness of structures may be measured through the ratio of the toughness of the material G_F to the product of its strength f_t and of the maximum size of the structure D. This ratio is a pure number, with no physical dimension, and depends on the dimensional scale of the body. Based on this ratio, a small glass body and a large steel ship of same geometry may appear to be equally brittle, just as a thin steel body and a microscopic glass filament may appear equally ductile.

The variation in structural response as the size of the structure changes is called "ductile-brittle transition," and in recent years has led to a flourishing crop of theories and models capable of describing and reproducing this surprising phenomenon. As has always occurred in the history of science, there has been much discussion, at times heated, among researchers because of the fact that the new and general models must only simulate the transition, but must not contradict the most classic and by now firmly accepted facts. Material behavior laws have therefore been generalized to include, as limit cases, theory of plasticity on the one hand, and linear elastic fracture mechanics on the other. New mathematical theories concerning catastrophes [22] and fractals are also providing a useful contribution to the description and understanding of this phenomenon, which is irregular, discontinuous, and without any physical similitude as the scale changes.

The classic elastic-perfectly plastic constitutive law (Figure 6a) is obviously not appropriate for describing the localization of damage into a crack, nor brittleness, in the sense of a sudden structural unloading. Quite recently it has been pointed out how even the strain-softening constitutive laws (Figure 6b), which represent tension σ as decreasing with strain ϵ, are not suitable for simulating localization phenomena, especially for reproducing dimensional effects. Only a double constitutive law which uses stress and strain up to the maximum load, and stress and crack opening in the softening stage (Figure 6c) is useful for this purpose (cf. eq 1).

Let us consider three bars of the same material but of different lengths under tension (Figure 7a). While the stiffness of the bars decreases with length, peak-stress f_t and dissipated energy $W_d = G_F A$, where G_F = fracture energy and A = area of the cross-section, must

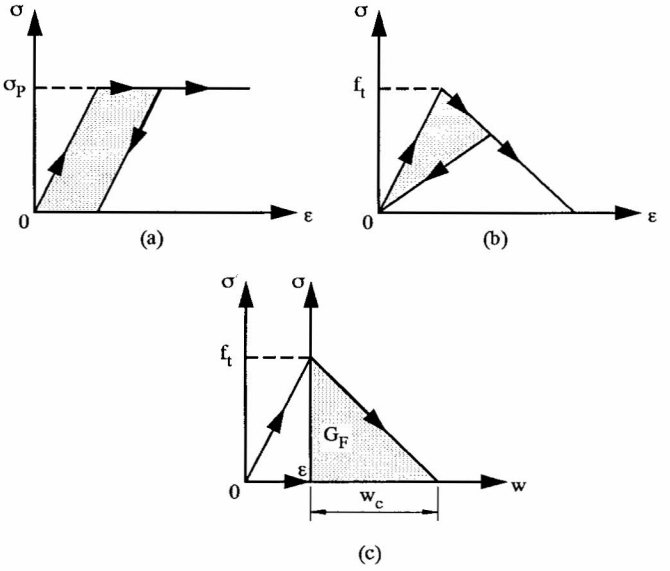

FIGURE 6. Material constitutive laws: (a) elastic perfectly plastic; (b) strain-softening; and (c) cohesive.

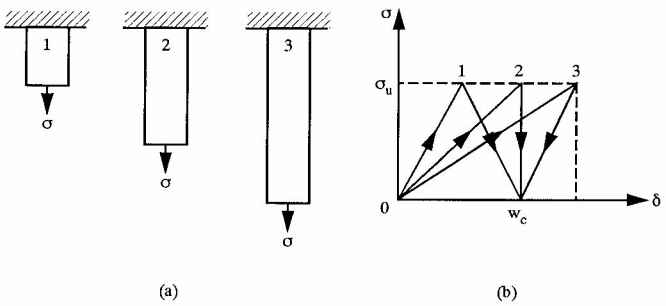

FIGURE 7. The response to uniaxial traction may be unstable or catastrophic depending on the length of the bar.

remain constant as the length changes (Figure 7b). This means that the triangle formed by the elastic branch, the softening branch, and the axis δ, where δ = total lengthening of the bar, must always have the same area as the length of the bar changes. The maximum elongation w_c (Figure 6c) must also be the same. Consequently, as soon as the stiffness of the bar falls below f_t/w_c, so that its length exceeds $\ell_o = Ew_c/f_t$, the softening branch takes on a positive slope and represents a particularly unstable failure phenomenon, called "snap-back." It is observed that for concrete with E = 30, GPa, $w_c = 10^{-4}$ m, $\ell_o = 1$ m. When the snap-back branch is present, failure occurs in a catastrophic manner even if controlled by the displacement δ. Once the value of δ relative to the peak stress f_t has been reached, the loading capacity immediately falls to zero and the bar snaps.

The same transition from ductile to brittle response takes place even in structures of complex form as the dimensions increase but the geometric ratios remain unchanged (geometric similitude). Figure 8 shows the load-deflection response of samples from a polymeric material, subjected to three-point bending. Note how no physical similitude in failure behavior appears as the size changes. Sudden failures, with large energy release and rapid crack propagation, whether or not any cracks existed before the test, may all be interpreted through a virtual snap-back branch which is not traversed in a stable manner, but rather "jumped" by the point representing the system (Figure 9). These occur with materials having relatively low fracture energy and relatively high tensile strength, in addition to large structural sizes. It is not the individual values of G_F, f_t, and D (D = characteristic dimension of the structure) that determine the degree of brittleness or ductility of geometrically similar structures, but their nondimensional function known as the brittleness number [23],

$$s_e = \frac{G_F}{f_t D} \tag{7}$$

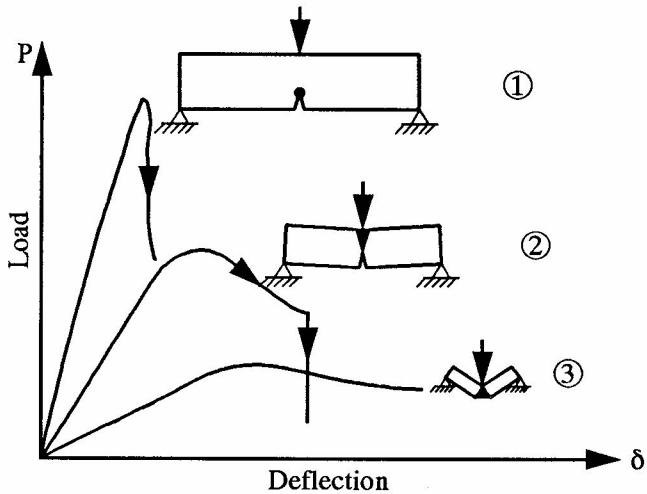

	Structural Behaviour	Crack Growth Process
①	Brittle	Unstable
②	Ductile-Brittle	Stable-Unstable
③	Ductile	Stable

FIGURE 8. Ductile-brittle dimensional transition in three-point bending tests.

although it is not quite clear yet as to why exactly this combination of parameters should describe the ductile-brittle transition so well.

In a flexed beam, the crack opening w is not uniform, but increases away from the tip of the crack itself (Figure 10a). In agreement with the σ–w diagram of Figure 6c, the interaction between the opposite faces of the crack decreases away from the tip, until it vanishes at $w = w_c$ (Figure 10b). The constitutive model in Figure 6c is thus correlated to the cohesive crack model, which is schematically represented in Figure 10b. This model predicts a softening structural response, which exhibits the same size effect as illustrated earlier for the

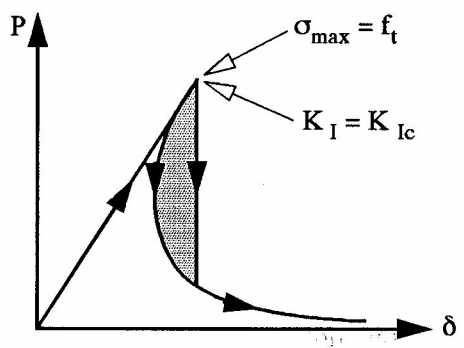

FIGURE 9. Virtual snap-back branch and vertical drop in the loading capacity if the controlling parameter is the deflection δ.

Advn Cem Bas Mat
1993;1:92–105

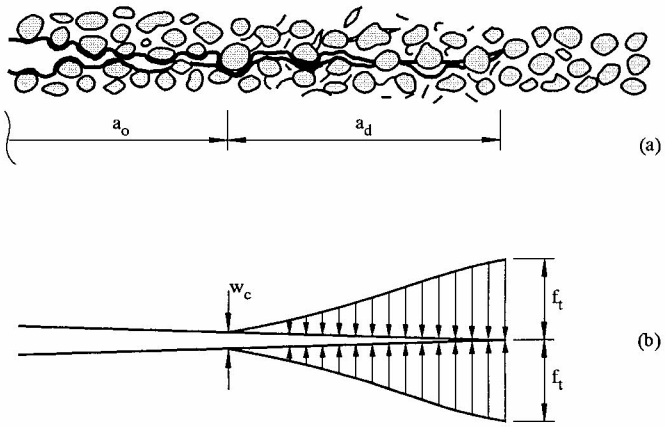

FIGURE 10. (a) Crack in the flexural concrete element; (b) cohesive crack model (cf. Figure 3).

uniaxial tension test. As the initial depth of the crack, a_o/D increases, a decrease in stiffness and loading capacity is observed, as well as an unexpected increase in ductility (Figure 11a). As G_F decreases to a value more characteristic for mortar than for plain concrete (Figure 11b), the various tendencies remain, but the system appears to be much more brittle—so much indeed that the snap-back phenomenon occurs for $a_o/D \leq 0.25$. For $a_o/D = 0$, that is, for an initially uncracked beam, the cusp is especially sharp and implies an explosive release of kinetic energy.

If instead the material is kept unchanged, say a concrete with $G_F = 50$ N/m, but only the depth scale is changed (with $\ell/D = 4$), one notices a considerable increase in brittleness as the beam depth D increases (Figure 12). As mentioned previously, all of these tendencies may be captured by changing only the nondimensional parameter s_e (eq 7). Figure 13 shows the structural responses considered earlier in a nondimensional form as s_e changes over four orders of magnitude. At the lower extremity of the range (curve A), one can find both especially brittle materials (low G_F/f_t ratio) and especially large beams (high value of D).

For the purpose of building safety, it is therefore very important to control the evolution of the mechanical damage processes, which, as we have seen, can be intrinsically stable, unstable, or catastrophic. The deformation of a loaded structure increases first in proportion to the load and then more rapidly as the stiffness reduces because of damage. Thus, as deformations increase beyond a certain level of damage, it is necessary to decrease the applied force to avoid sudden failure. This unstable damage stage may be kept under check by controlling the monotonically growing deformation but not by controlling the force, which must decrease. Often the unstable stage is followed by a third catastrophic stage when a macrocrack forms

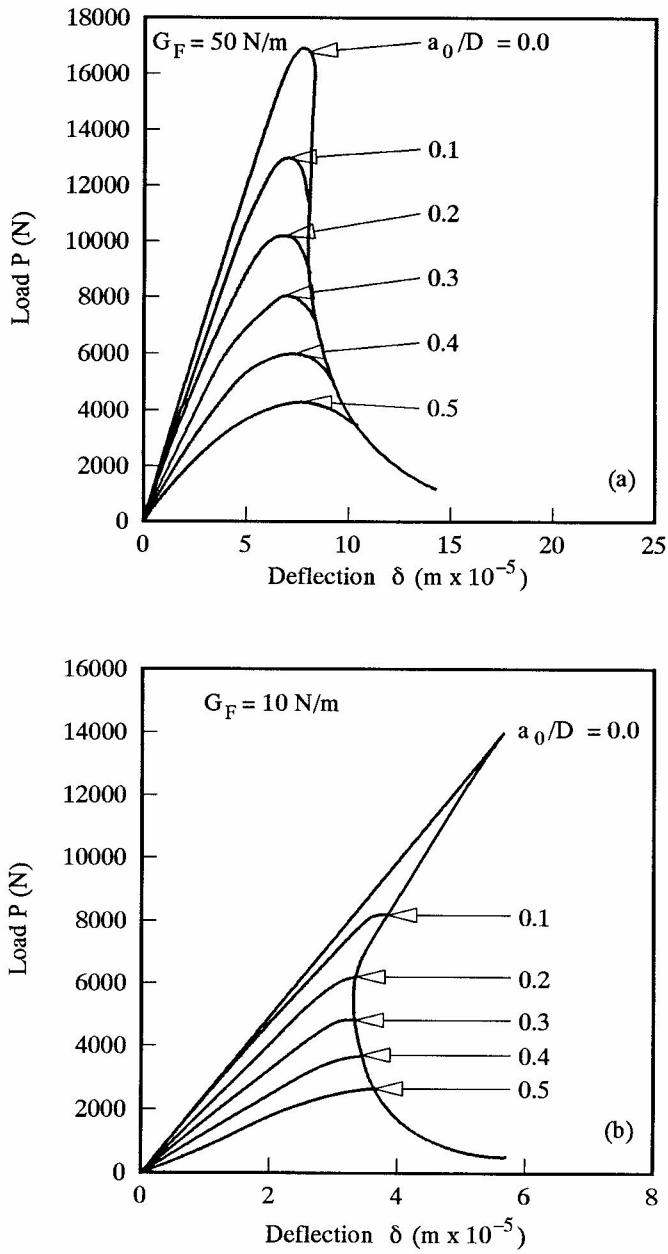

FIGURE 11. Structural load-deflection response as the depth a_0/D of the initial notch changes in a three-point bend beam.

and extends. While the crack separates the element into two distinct parts, the internal stresses relax and the deformations are reduced, just as the external force continues to decrease. The catastrophic stage can be kept under check by controlling the crack opening or extension as these are the only quantities which continue to increase (Figure 14). With the aid of modern automatic control techniques, it is therefore possible to observe a brittle failure "in slow motion." It is quite possible that what we are able to stabilize today in the laboratory, we will be able to do in practice in the

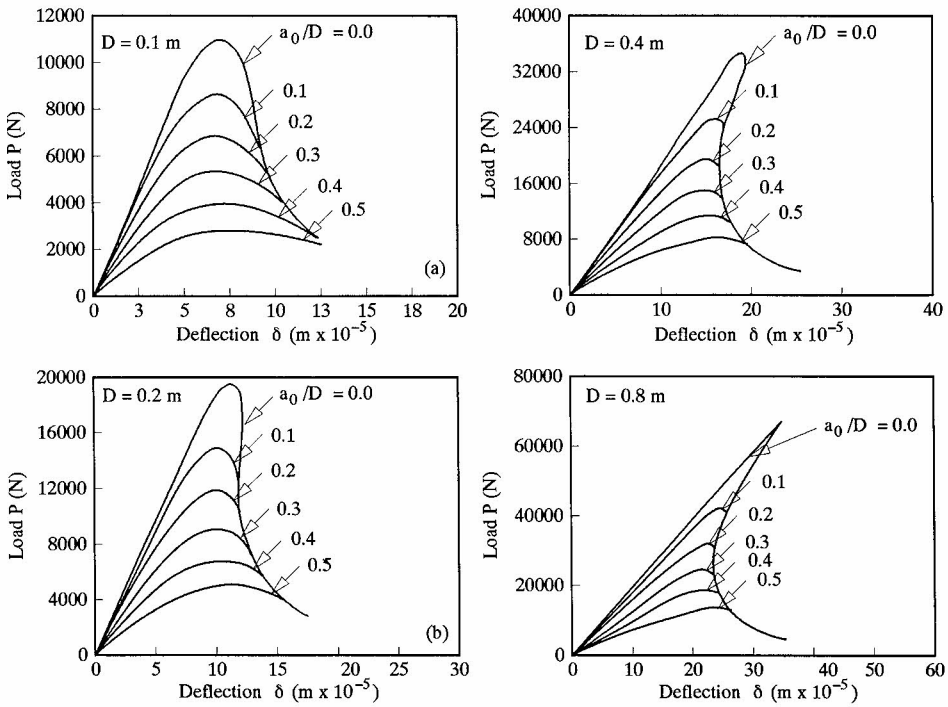

FIGURE 12. Structural load-deflection response as the dimensional scale changes.

future and be able to stabilize, or even stop, an imminent structural collapse.

Flexural Strength Size Effects

In this section, two-dimensional structures which are initially uncracked and with a unique growing cohesive macrocrack, are considered [24,25]. A slab in three-point bending is numerically simulated by varying the brittleness number s_e.

Several dimensionless load-deflection diagrams are plotted in Figure 13 for a concretelike material with ultimate tensile strain ϵ_u = 87 μm, Poisson's ratio ν = 0.1, t = D, ℓ = 4D, a_o/D = 0.0. The specimen behavior is brittle (snap-back) for a low fracture toughness G_F, high tensile strength f_t, and/or large sizes D. For $s_e \leqslant 10.45 \times 10^{-5}$, the P–δ curve has a positive slope in the softening branch, and a catastrophic event occurs if the loading process is deflection-controlled, which can be avoided if the loading process is controlled by a monotonically increasing function of time, for example, by the displacement discontinuity across the crack or by a linear combination of load and deflection [26]. When the postpeak behavior is kept under control up to complete rupture, the area under the load-deflection curve represents the product of the fracture energy G_F and the initial cross-sectional area Dt.

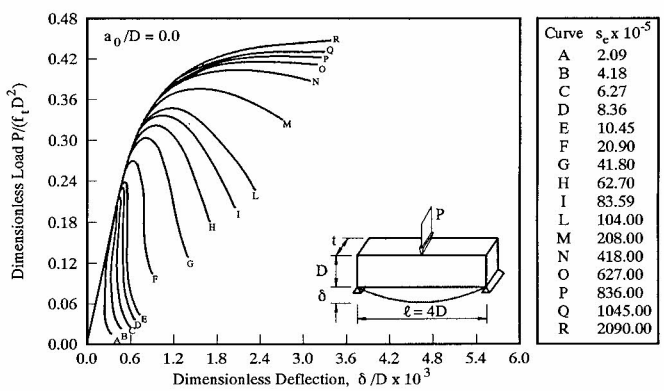

FIGURE 13. Structural load-deflection response as the brittleness number $s_e = G_F/(f_t D)$ changes.

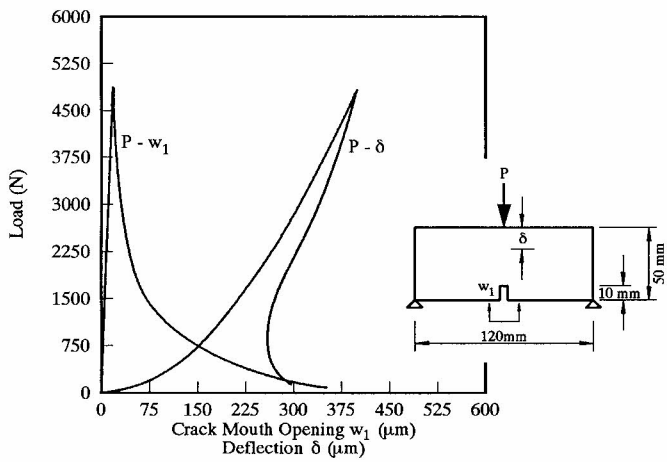

FIGURE 14. Stabilization of a catastrophic branch by controlling the crack mouth opening w_1.

Advn Cem Bas Mat
1993;1:92–105

The maximum loading capacity $P^{(1)}_{max}$ of initially uncracked specimens with $\ell = 4D$ is obtained from Figure 13, whereas the maximum load $P^{(3)}_{max}$ at the ultimate strength is given by

$$P^{(3)}_{max} = \frac{2}{3}\frac{f_t t\, D^2}{\ell}, \tag{8}$$

The ratio $P^{(1)}_{max}/P^{(3)}_{max}$ may also be regarded as the ratio of the apparent tensile strength f_a (given when the maximum load $P^{(1)}_{max}$ is substituted into eq 8) to the true tensile strength f_t (considered as material constant). It is evident from Figure 15 that the results of the cohesive crack model tend to those of the ultimate strength analysis for low s_e values, that is, $\lim_{s_e \to 0} P^{(1)}_{max} = P^{(3)}_{max}$. Therefore, $f_a = f_t$ only for comparatively large specimen sizes. With the usual laboratory specimens, an apparent strength higher than the true one is always found [27].

In the limit as $D \to 0$ or fracture energy $G_F \to \infty$ (elastic-perfectly plastic material in tension), that is, as $s_e \to \infty$, the apparent strength f_a tends to $3\, f_t$.

There are similar size effects in the indirect tensile strength (split strength) of quasibrittle materials, but their description is beyond the scope of this article.

R-Curve Approach to Fracture of Cementitious Materials

Linear Elastic Approximation of the Cohesive Crack

In the preceding sections, the cohesive crack concept was shown to be useful for the discussion of the ductile-brittle transition. Nevertheless, its implementation is not straightforward. A simplified procedure to study crack growth in cement mortar and plain concrete is based on the equivalent elastic crack concept and its associated *R*-curve. One such elastic equivalence was already pointed out in the section on Effective Griffith Crack Concept. Like all simplifications, it has limitations that are worth examining.

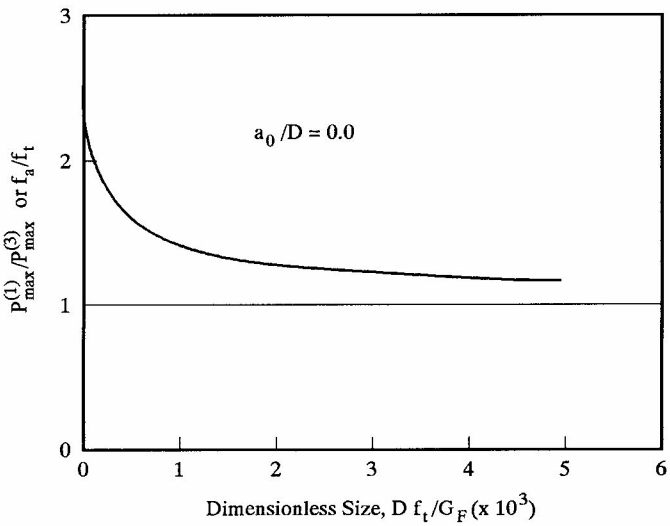

FIGURE 15. Decrease in apparent flexural strength with increasing specimen size.

The use of crack growth resistance curves (R-Δa) to predict the behavior of cracked specimens is a well-established practice for ceramic, cementitious, and other quasibrittle materials (see, e.g., ref 28). Assuming that the cohesive crack model can be applied to these materials, it will be shown that the use of R-Δa curves is equivalent to setting up an elastic equivalence between the actual (cohesive)specimen and a fictitious (linear elastic) one.

A further reason for exploring how far a cohesive crack can be treated as a linear elastic one is the use of the fracture toughness concept—K^e_{Ic} or K^s_{Ic}—for the quasibrittle materials. When the design is based on K^e_{Ic} or K^s_{Ic}, it is quite obvious that this value should be a material property to predict the behavior of a component from a value extracted from a particular specimen tested in a laboratory. Consequently, the validity and significance of this concept is by no means clear unless an acceptable degree of linear elastic behavior is proven.

The equivalent elastic crack greatly simplifies the computations by shifting from a cohesive material (and hence a nonlinear structural analysis) to a linear elastic material (which only requires linear analysis). But as already mentioned, this simplification is not always acceptable and a discussion of its suitability and range of its validity is the objective of this section. The unified concept of equivalent elastic crack, as described in this section, was developed by Elices and Planas et al. in several articles [29–32], and some of their results are summarized here.

First, the more familiar equivalences based on load, the so-called P–Y equivalences, are reviewed and then the general X–Y equivalences are considered. It should be remarked that the discussion to follow is valid only for materials which can be modeled with cohesive cracks, that is, the experimental values should coincide with numerical computations using a cohesive crack model.

Load -Y Equivalences

The concept of elastic equivalence is best illustrated on a particular example. Let us choose the force-crack mouth opening displacement equivalence or P-CMOD equivalence, as in the two-parameter model [16]. As shown in Figure 16, two geometrically identical cracked samples are loaded under CMOD control. One sample is made from a cohesive material and the other

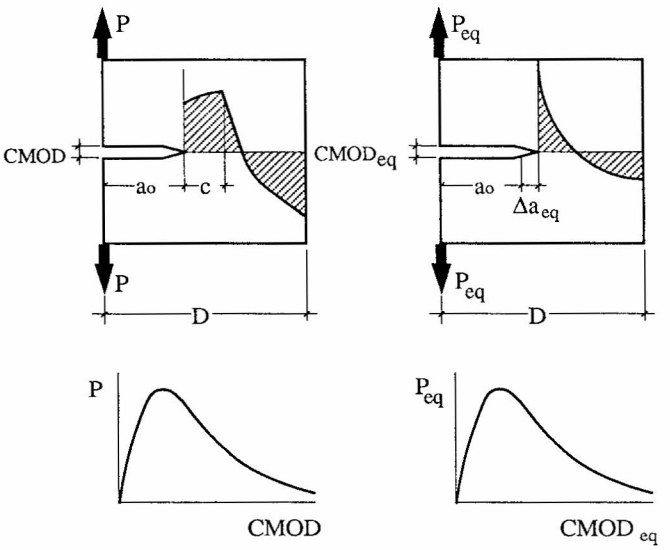

FIGURE 16. Force-crack mouth opening displacement (P-CMOD) equivalence.

(the equivalent) from a linear elastic material. The measured loads in the two samples—P and P_{eq}—for the same crack mouth opening displacement CMOD will be in general different, but we can force the loads to match each other ($P = P_{eq}$)—at each value of CMOD—by choosing a suitable equivalent crack length a_{eq} and a suitable equivalent crack growth resistance R_{eq}.

In this way we force both samples to exhibit the same P-CMOD behavior, but generally the equivalence ends here; stress fields, for example, need not be the same, as seen on Figure 16. The price paid for the forced equivalence is that the linear elastic material does not have a constant toughness (G_F for cohesive material) but rather a changing resistance—an R-Δa curve. What is worse is that this R-Δa curve is not a material property but depends on the geometry and specimen size.

For computing the R-Δa curve we proceed as follows. First, the equivalent elastic crack length is deduced. From the measured P and CMOD values in the cohesive sample, the equivalent elastic crack length a_{eq} is derived from the expression of the compliance for the equivalent elastic sample C_{eq} (a_{eq}) = CMOD/P. Then, the corresponding stress intensity factor is computed from LEFM

$$K_{Ieq} = \frac{P_{eq}}{B\sqrt{D}} S\left(\frac{a_{eq}}{D}\right) \tag{9}$$

where B is the specimen thickness, D is one of its characteristic in-plane dimensions, and $S(a/D)$ is the geometrical shape factor. Finally, the R-Δa curve is established from the well-known relation

$$R(\Delta a_{eq}) = \frac{1}{E'} [K_{Ieq}(P_{eq}, a_0 + \Delta a_{eq})]^2 \tag{10}$$

where the equivalent crack length was written explicitly as $a_{eq} = a_o + \Delta a_{eq}$ to emphasize its dependence on the crack increment, and E' is the generalized elastic modulus ($= E$ in plane stress, or $= E/(1 - \nu^2)$ in plane strain). Notice that this R-Δa curve is dependent on the size and geometry of the specimen because of the implicit size and geometry dependence of Δ_{eq}.

As an example of the application of the load-CMOD equivalence, imagine we want to predict the load-CMOD of a cracked panel in tension (CPT) made from a cohesive material using test results of a three-point notched beam (TPB) made of the same material. These two different geometries are chosen because the loading of the respective uncracked ligaments is quite different; flexural loading in the beam ligament and tensile loading in the panel. Figure 17 shows the geometry of the specimens and the assumed softening function of the cohesive material.

The procedure, based on the R-curve approach, to compute the load (P)-CMOD is as follows: The P-CMOD is first measured from TPB test, from which the corresponding R-Δa curve is derived. Then, assuming that the R-curve is a material property, a P-CMOD curve for the notched panel is predicted under the additional assumption of linear elastic behavior. As we shall see later in this section, the accuracy of the pre-

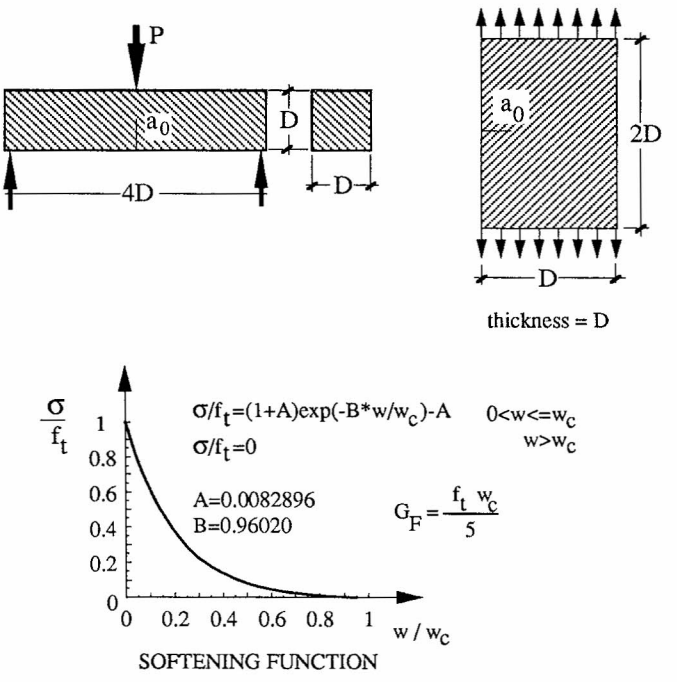

FIGURE 17. (a) Reference beam and notched panel geometries; and (b) softening function.

diction depends on the validity of these two assumptions.

As the experimental values are assumed to be indistinguishable from the numerical computations based on cohesive cracks, the measured (computed) P-CMOD curve for the TPB is as shown in Figure 18a for $D = l_{ch}$ (where $l_{ch} = EG_F/f_t^2$) and $a_o = 0.5D$, and the resistance curve, $R\text{-}\Delta a^{P\text{-}CMOD}$, of the equivalent elastic beam computed according to the above procedure is as depicted in Figure 18b. The prediction under the above assumptions of P-CMOD is shown in Figure 19a together with the experimental results. That the prediction is very close to the experimental results is because the R-curves of the beam and the panel are very similar for the sizes and relative notch depths considered, as shown in Figure 19b.

If the relative sizes and notch depths are different there is no reason why a good agreement should result, as is clear from Figure 20 for a panel with $D = 31_{ch}$ and $a_o = 0.1D$, which has been computed based on the R-Δa curve derived from the small beam (Figure 18b).

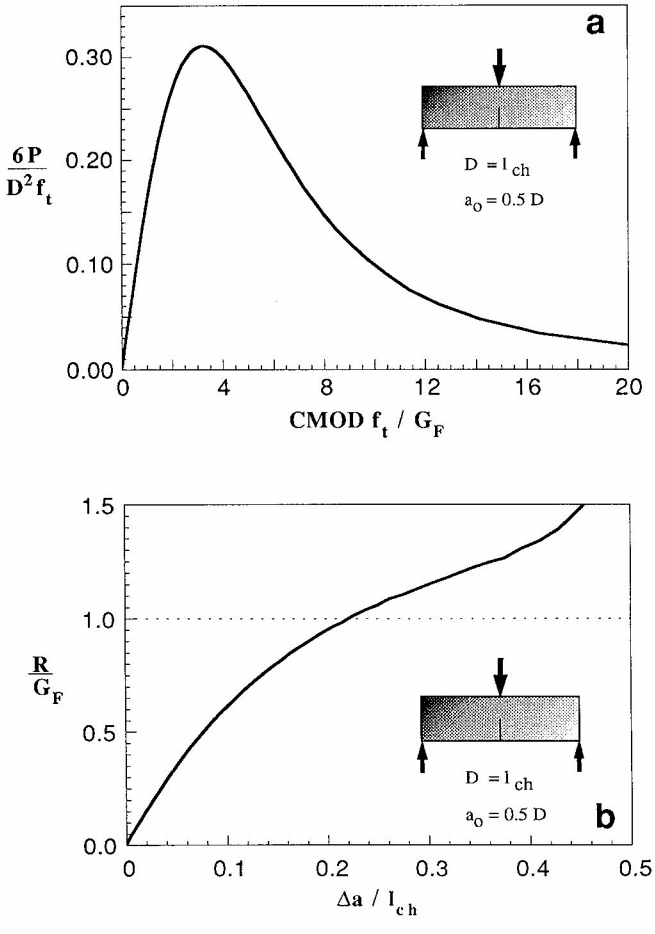

FIGURE 18. Reference beam (a) measured P-CMOD values; and (b) corresponding R-Δa curve (for P-CMOD equivalence).

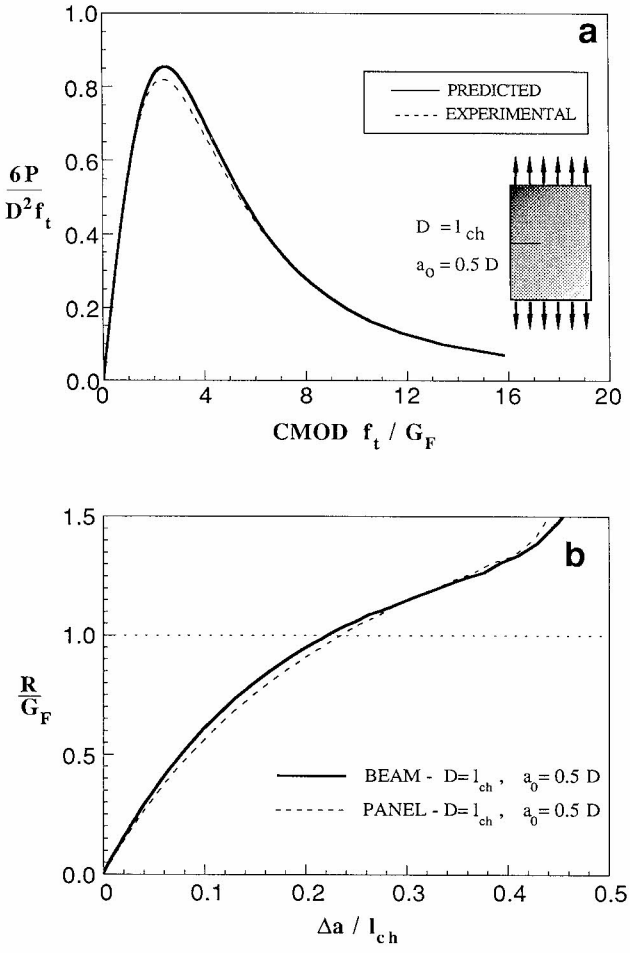

FIGURE 19. Prediction for a notched panel using a P-CMOD equivalence: (a) P-CMOD curves (predicted and experimental); and (b) R-Δa curves (TPB reference and corresponding CPT curve).

Apart from the P-CMOD equivalence, other P-Y equivalences may be sought (where Y stands for other possible magnitudes). For example, when the displacement u in the load-displacement record is chosen as a second variable, one arrives at the load-displacement equivalence, P-u equivalence. If the second variable is the crack tip opening displacement, the P-CTOD equivalence results. Also, a P-J equivalence may be considered when information about the softening behavior of the cohesive material is known. All these equivalences are analyzed in detail in ref 31.

The corresponding crack growth resistance curves need not be the same. Figure 21a shows the computed R-Δa curves for a TPB ($D = l_{ch}$, $a_o = 0.5D$) for the three equivalences P-CMOD, P-u, and P-J. Although they do not coincide, the shapes are similar for small crack extensions, so that similar outputs can be expected regardless of the type of equivalence, as is seen from Figure 21b. The main difference between the

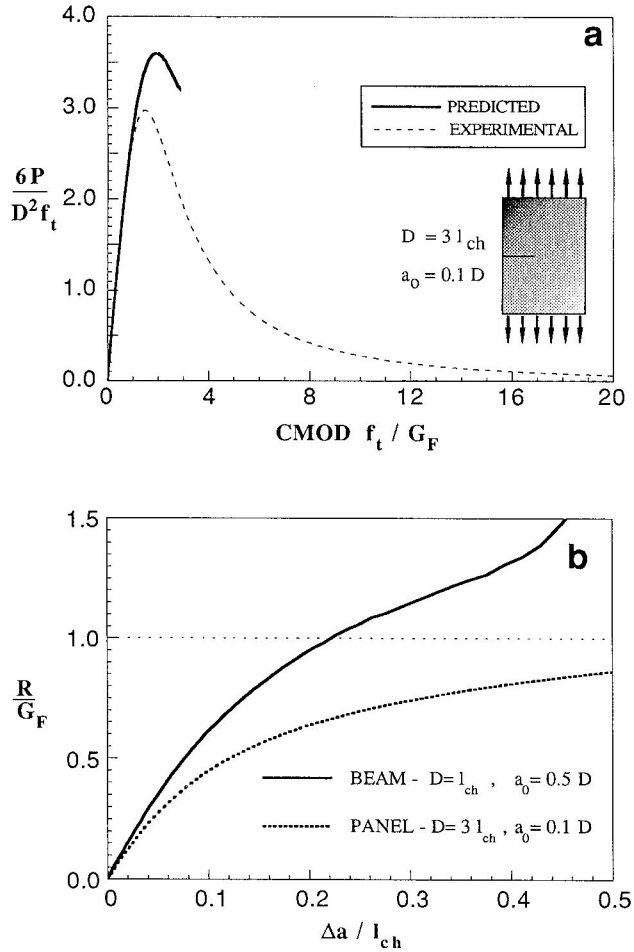

FIGURE 20. Prediction for a notched panel using a P-CMOD equivalence: (a) P-CMOD curves (predicted and experimental); and (b) R-Δa curves (TPB reference and corresponding CPT curve).

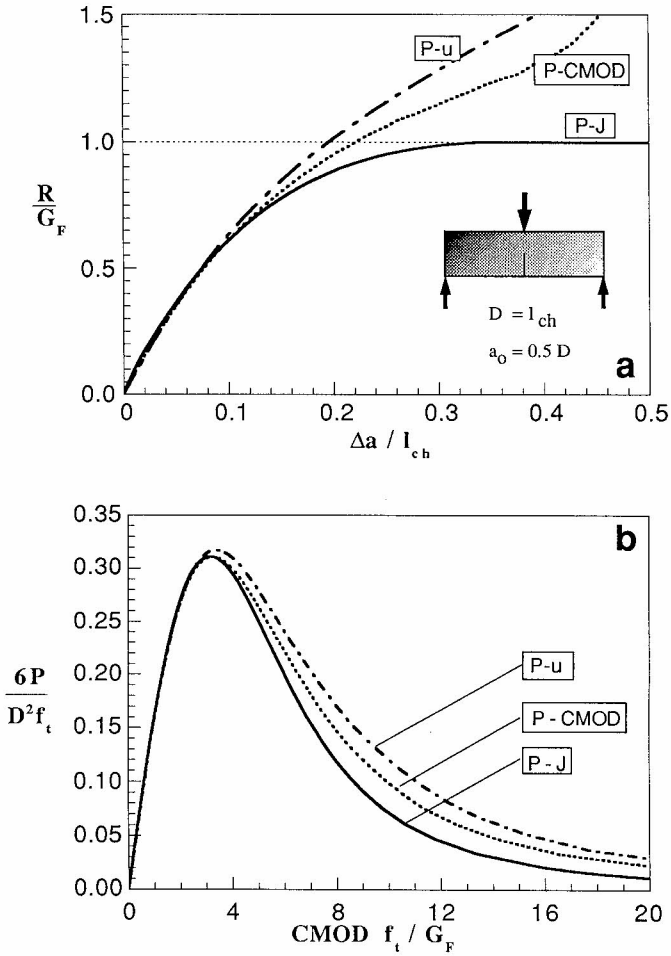

FIGURE 21. Comparison of different equivalences: (a) R-Δa curves for TPB for three equivalences; and (b) P-CMOD curves for the three equivalences. Notice that, by definition, the P-CMOD curve "predicted" by the P-CMOD equivalence exactly coincides with the "experimental" P-CMOD curve.

P-CMOD, *P-u* equivalences, and the *P-J* equivalence appears at large crack extensions because the *P-J* equivalence does not induce crack arrest when it reaches the free surface, but it is of no practical consequence [30].

For large specimens, the linear elastic equivalence may be useful for the following reasons: for cohesive materials it was shown [29,33] as the specimen size increases the crack resistance curve tends toward an asymptotic limit that is independent of the specimen geometry (besides, of course, size) and depends solely on the shape of the softening function. For the quasiexponential softening function chosen for these examples, the asymptotic R-Δa curve is shown in Figure 22a. The point of tangency of the rising R curve with the horizontal branch ($R/G_F = 1$) happens at $\Delta a_{e\infty}^{\text{P-CMOD}} \approx 2.48\ l_{ch}$ [29]. Here, $\Delta a_{e\infty}^{\text{P-CMOD}}$ is the equivalent crack extension for infinite specimens at peak load. Also shown on Figure 22 are two R-Δa curves corresponding to two large specimens of quite different geometry; a TPB ($D = 6\ l_{ch}$ and $a_o = D/6$) and a CPT ($D = 6\ l_{ch}$ and $a_o = 0.1D$). It is seen that both curves are very similar (except near the very end) and tend to merge with the asymptotic curve.

Results of P-CMOD curves for the CPT panel are shown in Figure 22b using the references beam (TPB) and the asymptotic R curve. For comparison, the experimental values are also shown. These results show that it is possible to compute accurate values of the maximum loads and of the shape of the P-CMOD curve using the equivalent elastic crack concept when samples are sufficiently large.

The asymptotic behavior of the P-CMOD equivalence may serve as a guide for discussing the asymptotic behavior of other equivalences. In this respect it is convenient to compare the equivalences based on variables associated with fields far away from the cohesive zone [29]. The variables P, CMOD, u, and J used to

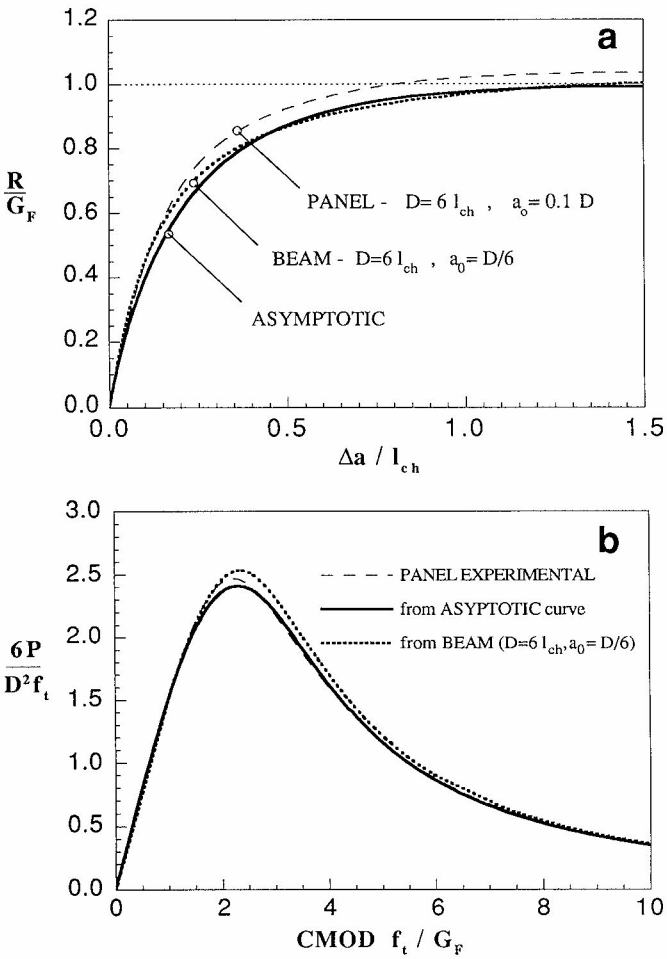

FIGURE 22. Predictions for the large notched panels, using a P-CMOD equivalence: (a) R-Δa curves for the large specimens; and (b) P-CMOD curves for a CPT specimen predicted from the TPB R-Δa curve and the asymptotic R-Δa curve. Experimental values are also shown.

define equivalences are far field variables. In references 29 and 33 it is shown that the equivalences based on far field variables merge into a single one for very large sizes. In particular, the far field crack extensions for the different equivalences (for the same softening function) are the same, that is,

$$\Delta a_\infty^{FF} = \Delta a_\infty^{\text{P-CMOD}} = \Delta a_\infty^{P\text{-}u} = \Delta a_\infty^{P\text{-}J}, \tag{11}$$

so that all R-Δa curves will tend toward a unique R-Δa curve for very large sizes, irrespective of the geometry considered. This curve will still depend on the softening properties of the cohesive material [29]. From this it follows that the predictions for large sizes will be the same irrespective of the chosen elastic equivalence, so long as it is based on a far field variable. When the variable is a near field one, such as the crack tip opening displacement CTOD, the general trend is still the same, but the asymptotic R-Δa curve does not coincide with the far field equivalents [33].

X-Y Equivalences

The concept of P-Y equivalence can be generalized to any controlling variable, not necessarily the load, P. The procedure used for P-Y equivalences can be extended to any pair of variables X-Y. This generalization will allow us to consider within the same framework apparently unrelated procedures, such as Bažant's R-Δa approach [34] or the J-CTOD approach [32].

The cohesive and the equivalent (linear elastic) specimens are not now bearing the same load, in general, and the equivalent $P^{X\text{-}Y}$ and equivalent crack length $a^{X\text{-}Y}$ corresponding to the elastic equivalent specimen can be computed by equating X and Y of the two specimens

$$X_{eq}(P^{X\text{-}Y}, a^{X\text{-}Y}) = X \tag{12}$$

$$Y_{eq}(P^{X\text{-}Y}, a^{X\text{-}Y}) = Y \tag{13}$$

where the right-hand members are the actual values of X and Y (either measured or computed using the cohesive model).

Equations 12 and 13 determine the equivalent load and crack length from which any other quantity can be found for the equivalent specimen. In particular, the equivalent crack growth resistance curve R-Δa is obtained from

$$\Delta a = a^{X\text{-}Y} - a_o \tag{14}$$

$$R(\Delta a) = \frac{1}{E'} [K_1(P^{X\text{-}Y}, a_o + \Delta a)]^2 \tag{15}$$

Further details may be gleaned from refs 32 and 33.

Acknowledgments

The financial support of the Australian Research Council to B.L. Karihaloo, that of the National Research Council and the Department for University, Scientific and Technological Research to A. Carpinteri, and of Dirección General de Investigación Cientifica y Técnica (MAT-92-0031) to M. Elices is gratefully acknowledged by the respective recipients. M. Elices also acknowledges fruitful discussions with the co-author of all his articles Professor J. Planas, related to the equivalent elastic crack concept.

References

1. Breslar, B.; Wollack, E. *Shear Strength of Concrete;* Report of the Department of Civil Engineering, University of California, Berkeley, 1952.
2. Kaplan, M.F. *J Am. Concr. Inst.* **1961,** *58,* 591–610.
3. Walsh, P.F. *Indian Concr. J.* **1972,** *46,* 469–476.

4. Walsh, P.F. *Mag. Concr. Res.* **1976,** *28,* 37–41.
5. Hillerborg, A.; Modéer, M.; Petersson, P.E. *Cem. Concr. Res.* **1976,** *6,* 773–782.
6. Kaplan, M.F. *J. Am. Concr. Inst.* **1963,** *50,* 853–880.
7. Karihaloo, B.L.; Fu, D. *Eur. J. Mech. A/Solids* **1989,** *8,* 373–384.
8. Horii, H.; Hasegawa, A.; Nishino, F. *Fracture of Concrete and Rocks;* Shah, S.P.; Swartz, S.E., Eds.; New York: Springer-Verlag, 1989; pp 205–219 (first presented at the Int. Conf. Houston, 1987).
9. Ortiz, M. *Int. J. Solids Struct.* **1988,** *24,* 231–250.
10. Melin, S. *Int. J. Fract.* **1983,** *23,* 37–45.
11. van Mier, J.G.M.; Vonk, R.A. *Mater. Struct.* **1991,** *24,* 61–65.
12. Reinhardt, H.W.; Cornelissen, H.A.W.; Hordijk, D.A. *ASCE J. Struct. Engng.* **1986,** *112,* 2462–2477.
13. Karihaloo, B.L.; Fu, D.; Huang, X. *J. Mech. Mater.* **1991,** *11,* 123–134.
14. Li, V.C.; Huang, J. *Engng. Fract. Mech.* **1990,** *25,* 39–46.
15. Karihaloo, B.L.; Huang, X. *J. Mech. Mater.* **1992,** *13,* 257–275.
16. Jenq, Y.S.; Shah, S.P. *ASCE J. Engng. Mech.* **1985,** *111,* 1227–1241.
17. Nallathambi, P.; Karihaloo, B.L. *Mag. Conc. Res.* **1986,** *28,* 67–76.
18. Karihaloo, B.L.; Nallathambi, P. *Fracture Mechanics Test Methods for Concrete;* Shah, S.P.; Carpinteri, A., Eds.; London: Chapman and Hall, 1991; pp 1–86.
19. Hillerborg, A. *Mater. Struct.* **1985,** *18,* 291–296.
20. Karihaloo, B.L. *Fracture Processes in Concrete, Rock and Ceramics,* Vol. I; van Mier, J.G.M.; Rots, J.G.; Bakker, A., Eds.; London: E & FN Spon, 1991; pp 163–172.
21. Karihaloo, B.L.; Nallathambi, P.; *Mater. Struct.* **1990,** *23,* 178–185.
22. Carpinteri, A. *J. Mech. Phys. Solids* **189,** *37,* 567–582.
23. Carpinteri, A. *Application of Fracture Mechanics to Cementitious Composites;* Shah, S.P., Ed.; Dordrecht: Martinus Nijhoff Publishers, 1985; pp 287–316; see also Carpinteri, A. *Engng. Fracture Mech.* **1982,** 467–481.
24. Carpinteri, A. *Int. J. Solids Struct.* **1989,** *25,* 409–429.
25. Carpinteri, A. *ASCE J. Engng. Mech.* **1989,** *115,* 1375–1392.
26. Rokugo, K.; Ohno, S.; Koyanagi, W. *Fracture Toughness and Fracture Energy of Concrete;* Wittmann, F.H., Ed.; New York: Elsevier, 1986; pp 403–411.
27. Petersson, P.E. *Crack Growth and Development of Fracture Zones in Plain Concrete and Similar Materials;* Report TVBMm 1006, Lund Institute of Technology, 1981.
28. Ouyang, C.; Shah, S.P. *J. Am. Ceram. Soc.* **1991,** *74,* 2831–2836.
29. Elices, M.; Planas, J. *Applications of Fracture Mechanics to Reinforced Concrete;* Carpinteri, A.; Ed.; London: Elsevier Applied Science, 1992; pp 169–200.
30. Elices, M.; Planas, J.; Guinea, G.V. *Fracture and Damage of Concrete and Rock;* Rossmanith, H.P., Ed.; London: E & FN Spon, 1993; pp 3–33.
31. Elices, M.; Planas, J. *Int. J. of Fracture* **1993,** *61,* 159–172.
32. Planas, J.; Elices, M. *Int. J. of Fracture* **1993,** *61.*
33. Planas, J.; Elices, M. *Int. J. of Fracture* **1992,** *55,* 153–177.
34. Bažant, Z. P.; Kim, J. K.; Pfeiffer, P.A. *ASCE J. Struct. Engng.* **1986,** *112,* 289–307.